Novel Wideband Circularly Polarized DRA With Squint-free Radiation Characteristics

Mohammad Abedian (m.abediankasgari@surrey.ac.uk)
Institute for Communication Systems (ICS), Home of the 5G & 6G Innovation Centres, University of Surrey, Guildford GU2 7XH, U.K.

Mohsen Khalily
University of Surrey

Vikrant Singh
University of Surrey

Pei Xiao
University of Surrey

Rahim Tafazolli
University of Surrey

Ahmed Kishk
Concordia University

Research Article

Keywords: circularly polarized dielectric resonator antenna (CP-DRA), rectangular dielectric resonator (RDRs) blocks, axial-ratio (AR) bandwidth

Posted Date: December 11th, 2020

DOI: https://doi.org/10.21203/rs.3.rs-124574/v1

Version of Record: A version of this preprint was published at Scientific Reports on March 30th, 2021. See the published version at https://doi.org/10.1038/s41598-021-86381-1.

Novel Wideband Circularly Polarized DRA with Squint-Free Radiation Characteristics

Mohammad Abedian[1,*], Mohsen Khalily[1], Vikrant Singh[1], Pei Xiao[1], Rahim Tafazolli[1], and Ahmed A. Kishk[2]

[1]Institute for Communication Systems (ICS), Home of the 5G & 6G Innovation Centres, University of Surrey, Guildford GU2 7XH, U.K.
[2]Department of Electrical and Computer Engineering, Concordia University, Montreal, QC H3G 2W1, Canada
[*]m.abediankasgari@surrey.ac.uk

ABSTRACT

A new single-fed circularly polarized dielectric resonator antenna (CP-DRA) without beam squint is presented. The DRA comprises of an S-shaped dielectric resonator (SDR) with a metalized edge and two rectangular dielectric resonator (RDRs) blocks. A horizontal-section is applied as an extension of the SDR, and a vertical-section is placed in parallel to the metallic edge. A vertical coaxial probe is used to excite the SDR and the vertical RDR blocks through an S-shaped metal element and a small rectangular metal strip, respectively. The two added RDRs that form an L-shaped DR improve the radiation characteristics and compensate for the beam squint errors. A wideband CP performance is achieved due to the excitation of several orthogonal modes such as $TE^{x}_{\delta 11}$, $TE^{y}_{1\delta 1}$, TE^{z}_{121}, TE^{y}_{112}, TE^{x}_{131}, and TE^{y}_{311}. The experimental results demonstrate an impedance bandwidth of approximately 66.8% ($3.71-7.45$ GHz) and a 3-dB axial-ratio (AR) bandwidth of about 54.8% ($3.72-6.53$ GHz) with a stable broadside beam achieving a measured peak gain of about $4.64\,dBi$. Furthermore, a 100% correction in beam squint value from $\theta = 41^{\circ}$ to $\theta = 0^{\circ}$ with respect to the antenna boresight is achieved.

Introduction

Dielectric resonator antennas (DRAs) have been widely studied due to their attractive features such as high radiation efficiency, low loss, no surface wave, various excitation mechanisms, light-weight, geometrical flexibility, and compact antenna size [1-3]. The 3D structure of DRAs provides a higher degree of flexibility over microstrip antennas that have been widely used in various systems but suffer from limited bandwidth and low radiation efficiency caused by the conduction losses [4]. Among the three main DRA shapes, rectangular DRA (RDRA) offers an added advantage of higher design flexibility as its three-dimensional structure can have different aspect ratios [5].

In addition, the amalgamation of various DRA shapes and coupling schemes provides the flexibility to obtain the desired linear or circular polarization (CP). Linear polarization (LP) is sensitive to multipath reception and misalignment between transmitting and receiving antennas. In contrast, CP waves, which are usually excited by two orthogonal linearly polarized waves of equal amplitude and 90-degree phase difference, have received much attention because they offer more flexibility for the transmitter and receiver orientations along with the capability of mitigating polarization mismatch and suppressing multipath interference [6-8]. Recently, different shapes of the DR along with various feeding mechanisms have been introduced to achieve wideband DRAs, operating in CP, as a pathway to fulfill spectrum requirements by taking the advantages of better mobility and less multipath effects [9-20]. To design circularly polarized DRA, two orthogonal modes must be excited with a quadratic phase difference, which can be realized by single or multiple feed mechanisms. The single feed mechanism has a relatively simple structure, but with limited CP bandwidth. Moreover, the radiation performance of the antenna can be degraded due to the asymmetry of the excitation. On the other hand, having a multiple feed network provides a wider CP bandwidth but results in a large and complex feeding structure. In the literature, several designs of single-point feed DRAs have been introduced to enhance the CP bandwidth [12-20]. For instance, in [12], a wideband CP quadruple-strip-fed cylindrical DRA with a CP bandwidth of 25.9% using a pair of 90° hybrid couplers has been presented. A trapezoidal DRA excited by an inclined slot has been proposed in [13], which offers a CP bandwidth of 21.5%. In [14], a DRA with diagonally inclined slits has been reported, which shows 43% AR bandwidth with an overlapped matching bandwidth of about 36%. Zou et al. [15] have introduced a RDRA excited by a spiral strip, achieving a CP bandwidth of 25.5%. In parallel, by exciting a RDRA through a unique conformal H-shaped metal strip, a wideband CP DRA with a CP bandwidth of 20% has been achieved [16]. Moreover, Yang et al. [17] proposed a square DRA excited by a microstrip coupled cross-slot with four vertical metal plates around the DRA, achieving a CP bandwidth of 46.9% with an average gain of $4.69\,dBi$ within the desired operating band. A

simple shaped RDRA with 20.8% AR bandwidth and high radiation efficiency of more than 97% has been presented in [18]. A DRA containing a rectangular and two half-split cylindrical DRs excited by a stair-shaped slot has been proposed in [19] which offers 41.01% AR bandwidth but low gain. A hybrid antenna with a cylindrical DR and dual vertical microstrip lines arranged perpendicularly for obtaining wideband CP bandwidth of 24.6% has been reported in [20]. However, it is observed that the radiation bandwidth is narrower than the matching bandwidth as the radiation characteristics changes within the desired bandwidth.

On the other hand, for a CP antenna, the antenna beam steering performance can be adversely affected by beam squint phenomenon resulting in displacement of the main beam and reduced antenna gain. Beam squint is caused by exciting higher order modes in the presence of the desired mode due to the asymmetry of the excitation as well as the geometry. Such squint is undesirable for communication as the peak amplitude in the co-component is not in the broadside direction. This behavior introduces frequency selectivity to the wideband signal, resulting in poor performance of the CP antenna and comprised system efficiency. Therefore, it poses a major limitation on its many practical applications, such as satellite and polarimetry [21]. One of the common techniques to excite orthogonal modes is to design an asymmetric resonator, but it may shift the main beam towards different angles rather than boresight. Furthermore, to widen the CP, the position of feeding structure with respect to the resonator plays an important role and can cause the deviation of the main beam from boresight. For example, the CP-DRAs in [14, 16, 18, 22-24] suffer from a large squint angle, which is more than 20° due to the asymmetry of the excitation and/or the resonator geometry. In this article, we have proposed a new technique to remove the beam squint effect and widen the CP bandwidth with radiation characteristic enhancement. The design procedure, as well as the measured and simulated results, will be discussed in the following sections.

Antenna Configuration and Physical Working Mechanism

The evolution and schematic of the proposed wideband CP-DRA is demonstrated in Fig. 1. Fig. 1(a) represents the initial design of the proposed DRA, where the CP bandwidth is limited to 4%. Hence, the RDR is modified to enhance the CP bandwidth by introducing two equal hollow blocks in RDR with the key parameters $l_{p2} = l_{p4}$ and l_2 to form an SDR (see Fig. 1(b)) to reduce DR's Q-factor and enhance impedance matching. Figure 1 (b), (c), and (d) illustrate three different geometries of the DRA denoted as Antenna I, Antenna II, and Antenna III, respectively. Fig. 1(d) depicts the final design of proposed DRA, indicating the design parameters, while Fig 1(e) presents the parameters associated with the feeding mechanism. For the purpose of achieving wideband CP, an SDR with dimensions $a_1 \times b_1 \times h_1$ excited by a coaxial probe through an S-shaped metal strip $l_p \times w_p$ (denoted as Antenna I. see Fig. 1(b)). The proposed DRA is supported by a grounded $26(x-axis)\,mm \times 26(y-axis)\,mm$ Rogers RO3003 substrate with a permittivity of $\varepsilon_s = 3$ and a thickness of $s = 0.75\,mm$. Secondly, a RDR with dimensions of $a_2 \times b_2 \times h_2$ is placed close to the SDR, excited by a small rectangular-shaped metal, $l_r \times w_r$, attached to the coaxial probe. In addition, a vertical metal strip with dimensions of $l_s \times w_s$ is placed on one side of the new resonator at a distance of l_d, resulting in a wider antenna bandwidth (denoted as Antenna II, see Fig. 1(c)). Finally, another RDR of volume $a_3 \times b_3 \times h_3$ is attached to the aforementioned DRs for improvement of the radiation characteristic (denoted as Antenna III, see Fig. 1 (d)). All the DRs are made of ECCOSTOCK® HiK dielectric material with relative permittivity $\varepsilon_r = 10$ and loss tangent $tan\,\delta = 0.002$.

In this work, CST Microwave Studio 2019 is used to analyze and optimize the proposed antenna. From a topological point of view, the main contribution of this work is exciting a single-fed CP antenna by applying an S-shaped parasitic strip attached to the DR block and, at the same time, compensating the beam squint error. It is worth noting that for further CP bandwidth improvement, two equal hollow blocks are introduced in the RDR. In parallel, two RDR blocks are placed to overcome the beam squint issue. In this section, we describe the design process of the proposed DRA and physical mechanisms.

Wideband CP-DRA design

As illustrated in Fig. 1(a), to couple the energy to the RDRA and excite multiple resonances in close vicinity, an S-shaped strip connected to the coaxial probe is attached to the RDRA while the initial dimensions of the RDRA are calculated using the dielectric waveguide model (DWM) equations [2]. Here, to generate CP fields, two orthogonal TE^x and TE^y modes with equal amplitude and 90° phase difference, are excited by using an S-shaped metal strip to indicate right-hand CP (RHCP) and left-hand CP (LHCP) waves components as follows [6]:

$$E_{RHCP} = \frac{1}{\sqrt{2}}\left(E_x + jE_y\right) \tag{1}$$

$$E_{LHCP} = \frac{1}{\sqrt{2}}\left(E_x - jE_y\right) \tag{2}$$

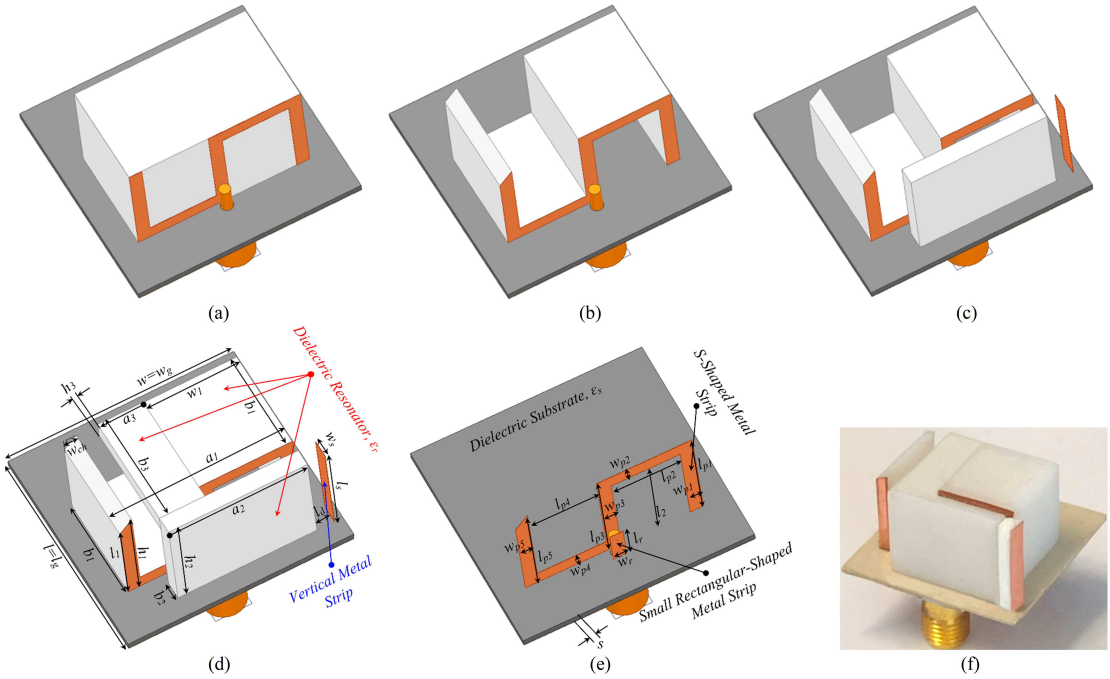

Figure 1. Evolution of the proposed CP DRA: (a) RDRA, (b) SDRA (Antenna I), (c) SDRA with the first added RDR and vertical metal strip (Antenna II), (d) SDRA with the first and the second added RDRs (Antenna III); Geometry of the proposed CP DRA, (e) feeding mechanism, and (f) the prototype of proposed DRA. ($l = l_g = 26$, $w = w_g = 26$, $l_{p1} = l_{p3} = l_{p5} = 12$, $l_{p2} = l_{p4} = 7.75$, $w_{p1} = w_{p3} = w_{p5} = 1.5$, $w_{p2} = w_{p4} = 2$, $l_r = 4$, $w_r = 2$, $l_s = 12$, $w_s = 2$, $l_d = 2$, $w_{ch} = 1.5$, $l_1 = 10.5$, $l_2 = 10$, $w_1 = 10.75$, $a_1 = 20$,$b_1 = 12$, $h_1 = 12$, $a_2 = 16$, $b_2 = 2$, $h_2 = 12$, $a_3 = 5.25$, $b_3 = 13.345$, $h_3 = 2$, $\varepsilon_r = 10$, $\varepsilon_s = 3$, $= 0.75$. $Unit : mm$).

According to image theory, the current of the S-shaped strip produces two distinct modes, common and differential, which correspond to exciting the TE^x and TE^y modes, respectively. The corresponding field components of each mode (TE^x and TE^y) are equal and can be expressed as follows [5]:

$$TE^x(E_y) = TE^y(E_x) = -AK_z\, cos(K_x x)\, cos(K_y y)\, sin(K_z z) \tag{3}$$

Figure 2 shows the simulated $|S_{11}|$ and AR of the RDRA with and without an S-shaped parasitic element. It can be clearly observed that the S-shaped strip provides wider impedance bandwidth with an overlapping broadside AR bandwidth around 4.1 GHz. In order to obtain a wider CP bandwidth, the RDRA is modified to form an SDRA. Fig. 3 shows the AR graph versus different values of $l_{p2} = l_{p4}$, at the resonance frequency of the corresponding first and second orthogonal mode pairs. It can be seen that as the length of $l_{p2} = l_{p4}$ increases, $3-dB$ AR bandwidth improves for the first and second orthogonal modes.

The SDRA provides a wider $3-dB$ AR bandwidth, as shown in Fig. 4. However, the corresponding impedance bandwidth shows a degradation and does not satisfy the $-10-dB$ $|S_{11}|$ around 6 GHz. To improve the impedance matching, a corner of the SDRA is chamfered with 45°, called Antenna I, as shown in Fig. 1(b). The simulated E-field distributions at 4.6 GHz and 6.5 GHz are shown in Fig. 5 for Antenna I. The figure indicates that orthogonal modes with equal magnitude and quadrature-phase are excited at both 4.6 GHz and 6.5 GHz. It is worth mentioning that the resonant modes excited across the desired CP band resemble orthogonal $TE^x_{\delta 11}$, $TE^y_{1\delta 1}$, TE^x_{131}, and TE^y_{311} modes.

Radiation characteristic improvement and beam squint reduction

Figure 6 illustrates the simulated H- and E-plane radiation patterns at 6.5 GHz for three different cases: Antenna I, Antenna II, and Antenna III, as shown in Fig. 1(b), (c), and (d), respectively. As for Antenna I, it is observed that the radiation pattern in the broadside direction deviates from the $+z$-direction with a high beam squinting of $-41°$, which does not satisfy the required specifications for CP antennas.

To fix the beam squint effect at 6.5 GHz, a RDR is placed in front of the SDRA to concentrate radiative fields toward boresight (see Fig. 1(c)). The RDR is excited by a small rectangular-shaped parasitic strip attached to the coaxial probe to improve the symmetry of the radiation patterns at the upper bands due to exciting higher-order modes inside the RDR. Another

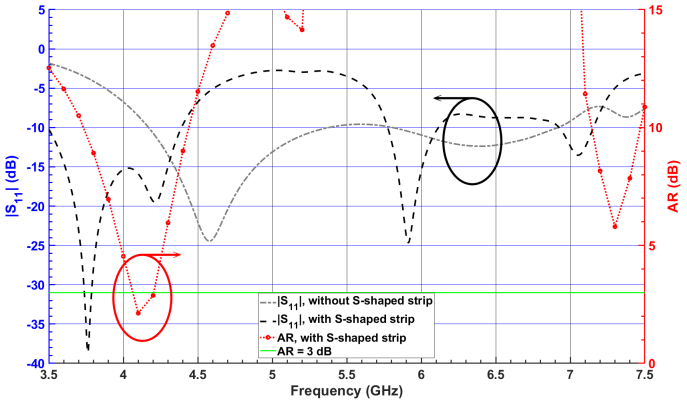

Figure 2. Simulated $|S_{11}|$ and AR of the RDRA with and without an S-shaped metal strip.

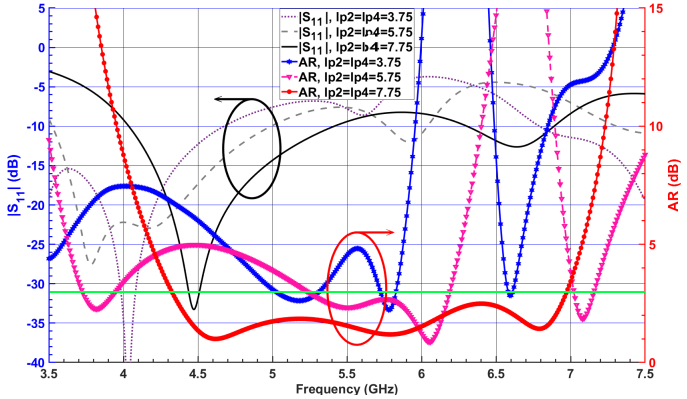

Figure 3. Simulated $|S_{11}|$ and ARs of the SDRA with different values of $l_{p2} = l_{p4}$.

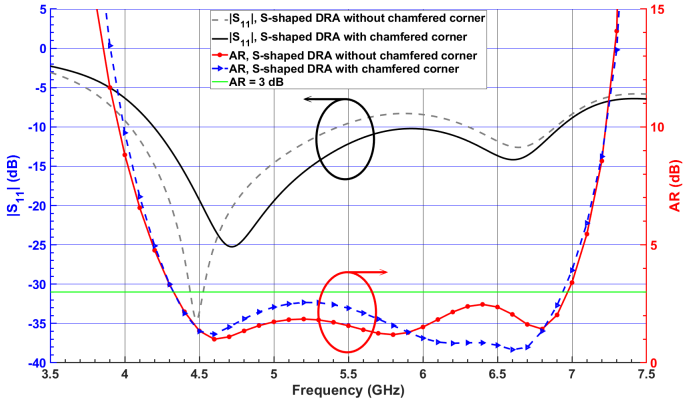

Figure 4. Simulated $|S_{11}|$ and ARs of the SDRA with and without chamfered corner.

important parameter that has a significant effect on the AR and $|S_{11}|$ is a_2. Fig. 7 illustrates the effect of varying a_2 on the AR and $|S_{11}|$, indicating that by increasing a_2, from $10\,mm$ to $18\,mm$, the higher edge of the bandwidth is increased. Besides, the separation between the corresponding resonant frequencies of the excited orthogonal modes inside the DRA increases the AR bandwidth. It is noticed that the beam squinting is reduced to 28°, which leads to an increased LHCP gain from $3.17\,dBi$ to $3.8\,dBi$ at 6.5 GHz. Then, a vertical metal strip is placed on one side of the thin RDR slab at a distance of $l_d = 2\,mm$, as illustrated in Fig. 1(c). By applying the vertical metal strip, the impedance matching, and CP bandwidth of the antenna is enhanced because of the increased effective resonator dimension in the x-direction. This leads to a downward shift in the resonant frequency of the corresponding higher-order modes [25], as shown in Fig. 8.

Finally, to further minimize the beam squint, the second RDR is horizontally attached to the aforementioned DR blocks in

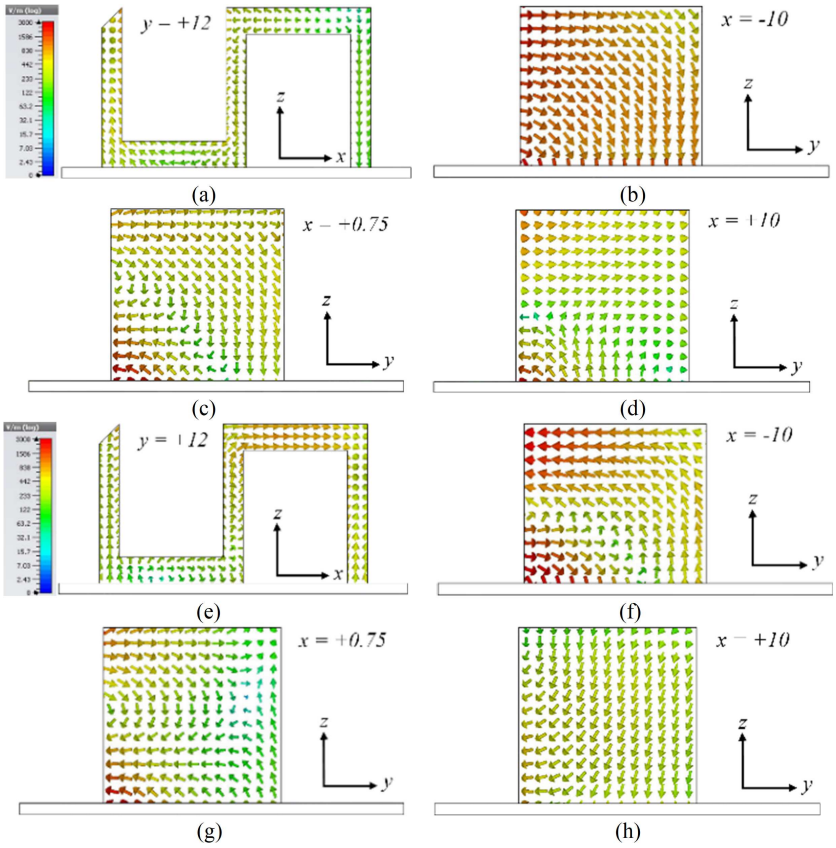

Figure 5. Simulated electric field vectors on different surfaces of the SDR; at 4.6 GHz (a) $\angle 45°(y = 12mm)$, (b) $\angle 135°(x = -10)$, (c) $\angle 135°(x = +0.75)$, and (d) $\angle 135°(x = +10)$; at 6.5 GHz (e) $\angle 45°(y = 12mm)$, (f) $\angle 135°(x = -10)$, (g) $\angle 135°(x = +0.75)$, and (h) $\angle 135°(x = +10)$; (color bar shows the amplitude of the E-field.

the y-direction, as shown in Fig 1(d). The effects of the second RDR with width a_3, on the antenna performance, is exhibited in Fig. 9. It is observed that the AR and $|S_{11}|$ are shifted down to the lower frequency as the width of the second RDR increases from $2mm$ to $6mm$. The widest overlapping bandwidth is achieved at $5.25mm$. Referring to Fig. 6, the boresight gain increases from $3.8dBi$ at $\theta = -28°$ to $4.7dBi$ at $\theta = 0°$ for 6.5 GHz frequency. It is noted that by applying the horizontal RDR, TE^z_{121} mode is excited inside the SDR, which is orthogonal to the existing TE^y_{112} mode excited within the first RDR, as shown in Fig.10. Furthermore, by increasing the effective resonator dimension in the y-direction, the total ratio of dominant orthogonal modes inside the DRA can be improved. This results in pattern rotation towards $\theta = 0°$ and gain enhancement. Based on this phenomenon, the $3-dB$ AR and impedance bandwidths shift down to the lower band, resulting in a wider impedance bandwidth of about 66.9% (3.66 – 7.34 GHz) and $3-dB$ axial-ratio (AR) bandwidth of about 54.54% (3.76 – 6.58 GHz).

Measured and Simulated Results

In this work, to reduce the complexity of design as well as fabrication difficulty two additional DR blocks are combined to form an L-shaped DR. Therefore, one S-shaped and L-shaped DR blocks are placed and fixed in the desired location to achieve satisfactory performance. In addition, a vertical metal strip is glued on a ROHACELL® HF Foam (ε_{ro} = 1.04) and then the L-shaped DR and foam are assembled on top of the substrate using RTV silicone adhesive ($\varepsilon_g = \approx 3$) to construct the CP DRA with a vertical metal strip.

S-parameter and axial ratio measurement

The simulated and measured frequency response of $3-dB$ AR and $|S_{11}|$ of the proposed antenna are depicted in Fig. 11, representing a close agreement between the simulated and measured results. The CP-DRA provides an impedance bandwidth of about 66.8% (3.71 – 7.45 GHz) and a $3-dB$ axial-ratio bandwidth of about 54.8% (3.72 – 6.53 GHz).

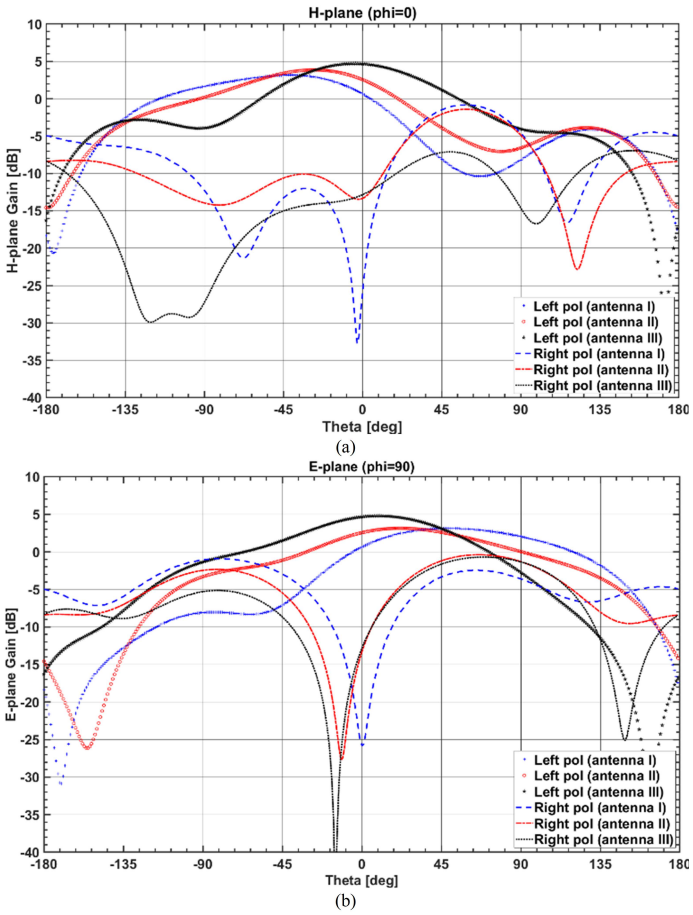

Figure 6. Simulated (a) H-plane and (b) E-plane radiation patterns of Antenna I, Antenna II, and Antenna III at 6.5 GHz.

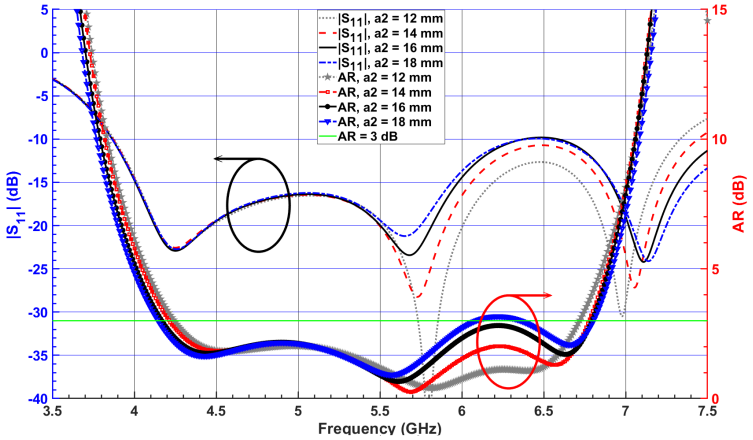

Figure 7. Simulated $|S_{11}|$ and ARs for the DRA (Antenna II) versus various total lengths a_2 of the first added RD.

Far-field measurement

Figure 12 illustrates the simulated and measured radiation patterns of the proposed DRA in xz-plane ($\phi = 0^\circ$) and yz-plane ($\phi = 90^\circ$). It can be seen that the proposed DRA's radiation patterns remain stable within the desired operating band. It can be observed from the figure that the difference between LHCP and RHCP radiation levels is more than $18\,dB$ confirming the purity of the LHCP radiation. Figure 13 shows simulated radiation efficiency along with the measured and simulated boresight gain of the proposed CP-DRA versus frequency. It is observed that a squint-free radiation pattern is obtained with a peak gain at boresight compensating the beam squint of 41°. The antenna efficiency remains at more than 97% throughout the passband of

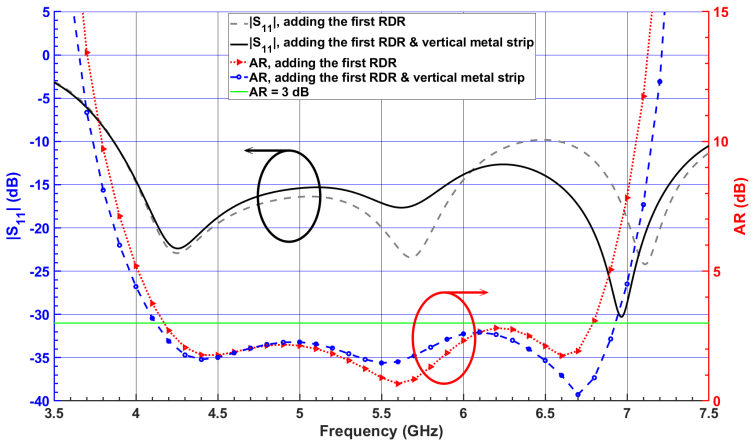

Figure 8. Simulated $|S_{11}|$ and ARs of the DRA (Antenna II), adding the first RDR block and vertical metal strip.

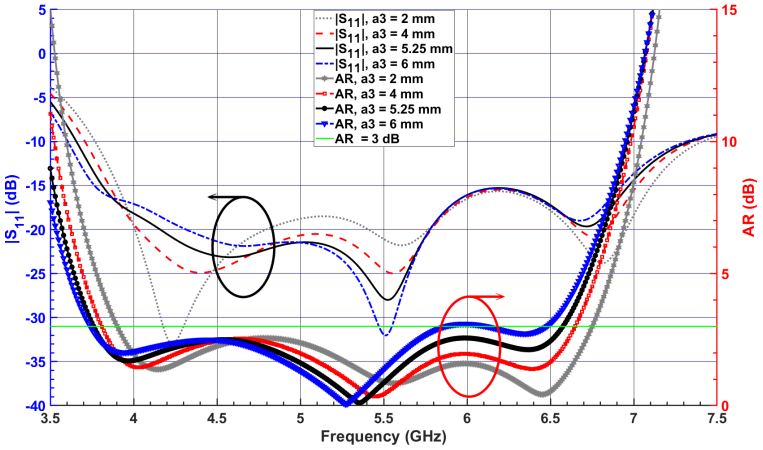

Figure 9. Simulated $|S_{11}|$ and ARs for the DRA (Antenna III) with various total widths a_3 of the second added RDR.

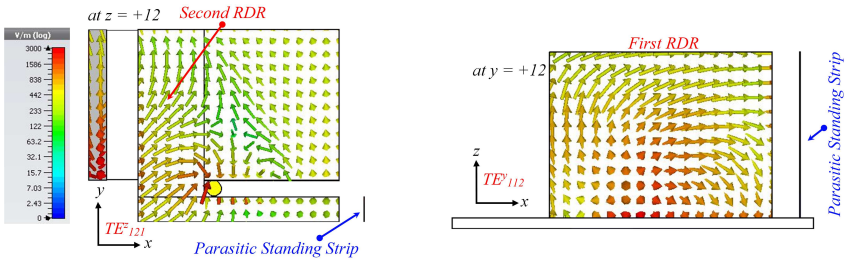

Figure 10. Simulated electric field vectors on the top surface of the SDR and the vertical surface of the first RDR at 5.5 GHz (a) xy-plane $\measuredangle 0^\circ (z = 12\,mm)$, (b) xz-plane $\measuredangle 90^\circ (y = 12\,mm)$; (color bar shows the amplitude of the E-field).

the DRA. Furthermore, the proposed antenna provides a gain of more than $2.85\,dBi$ within the desired $3-dB$ AR bandwidth with a peak gain of about $4.64\,dBi$.

Comparison with the state-of-the-art designs

Table I presents a comparison between the proposed CP-DRA and the previously reported designs, where λ_0 is the wavelength at the center frequency of the passband in free space. Compared to the state-of-the-art techniques reported in the literature, the proposed antenna offers a relatively wider AR bandwidth with squint-free radiations and a competitive trade-off between compactness and CP bandwidth.

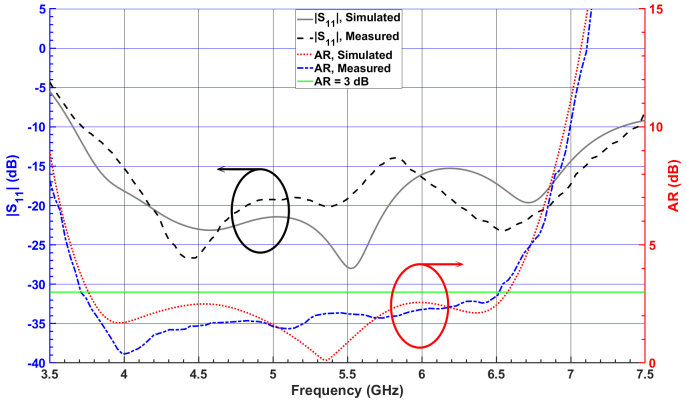

Figure 11. Simulated and measured $|S_{11}|$ and ARs of the proposed CP DRA.

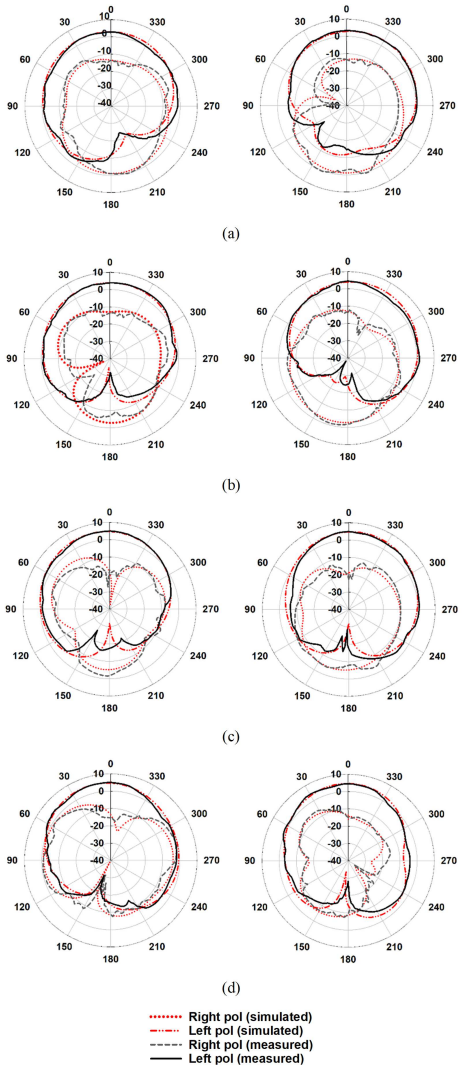

Figure 12. Simulated and measured LHCP and RHCP radiation patterns in *xz*-plane (left) and *yz*-plane (right) at (a) 3.76 GHz, (b) 4.6 GHz, (c) 5.5 GHz, and (d) 6.5 GHz. Red and black curves represent simulated and measured results, respectively.

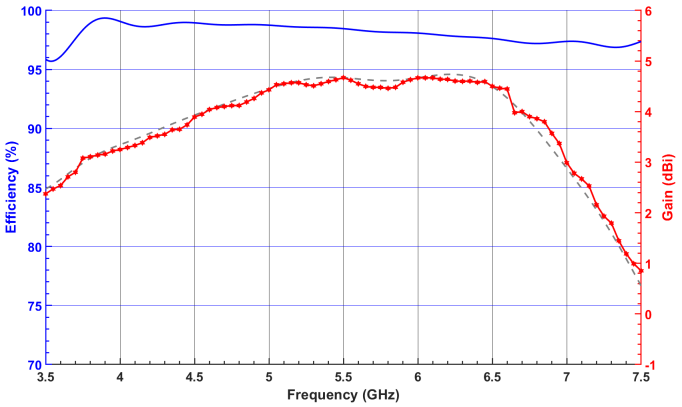

Figure 13. Measured and simulated boresight gain of the proposed CP-DRA and simulated radiation efficiency.

Ref.	ε_r	Antenna Dimensions (λ_0^3)	Imp. BW (%)	AR BW (%)	Peak Gain (*dBi*)
[14]	10	0.647×0.647×0.122	50.8	36	6
[15]	12	0.575×0.575×0.092	30.4	25.5	4.95
[16]	10	4.9×4.9×0.365	27.7	20	6.8
[17]	10	0.724×0.724×0.189	46.9	46.9	4.73
[18]	10	0.437×0.437×0.336	59.8	20.8	4.91
[19]	12.8	1.455×1.455×0.105	49.7	41	1.5
[20]	9.8	0.61×0.61×0.273	30.4	24.6	5.5
This work	10	0.484×0.484×0.237	66.8	54.8	4.64

Table 1. Comparison with CP DRAs in the literature.

Conclusion

A novel wideband circularly polarized DRA with squint-free radiation characteristics has been proposed. A 100% correction of beam squinting ($\theta = 41^\circ$) with respect to boresight has been obtained by loading two horizontally and vertically positioned RDRs (L-shaped DR). The experimental results have demonstrated that the proposed CP-DRA achieved about 66.8% (3.71 – 7.45 GHz) of matching bandwidth, which completely covers the $3-dB$ AR of about 54.8% (3.72 – 6.53 GHz) demonstrating its potential for various applications, such as compact communications, satellite communications, 5G Wi-Fi, WLAN, and WAP.

References

1. Luk, K. M. & Leung, K.W. (eds.). *Dielectric Resonator Antennas*, Baldock, England, Research Studies Press, (2003).
2. Leung, K. W., Lim, E. H. & Fang, X. S. Dielectric Resonator Antennas: From the Basic to the Aesthetic. *Proc. IEEE* **100**, 2181-2193 (2012).
3. Low, JH., Chee, PS., Lim, EH. et al. Compact organic liquid dielectric resonator antenna for air pressure sensing using soft material. *Sci. Rep.* **10**, 14907 (2020).
4. Petosa, A. & Ittipiboon, A. Dielectric Resonator Antennas: A Historical Review and the Current State of the Art. *IEEE Antennas and Propag. Mag.* **52**, 91-116, (2010).
5. Kumar Mongia, R. & Ittipiboon, A. Theoretical and experimental investigations on rectangular dielectric resonator antennas. *IEEE Trans. Antennas Propag.* **45**, 1348-1356 (1997).
6. Toh, B. Y., Cahill, R. & Fusco, V. F. Understanding and Measuring Circular Polarization. *IEEE Trans. Educ.* **46**, 313–318 (2003).
7. Steven Yang, S. L., Ricky Chair, Kishk, A. A., Lee, K. F. & Luk, K. M. Study on Sequential Feeding Networks for Sub-Arrays of Circularly Polarized Elliptical Dielectric Resonator Antenna *IEEE Trans. Antennas Propag.* **55**, 321-333 (2007).
8. Kaim, V., Kanaujia, B.K., Kumar, S. et al. Ultra-Miniature Circularly Polarized CPW-Fed Implantable Antenna Design and its Validation for Biotelemetry Applications. *Sci. Rep.* **10**, 6795 (2020).

9. Kishk, A. A. Elliptic Dielectric Resonator Antenna for Circular Polarization with Single Feed. *Microw. Opt. Technol. Lett.* **37**, 454-456 (2003).

10. Leung K. W. & Ng, H. K. Theory and experiment of circularly polarized dielectric resonator antenna with a parasitic patch. *IEEE Trans. Antennas Propag.* **51**, 405-412 (2003).

11. Chair, R., Kishk, A. A. & Lee, K. F. Aperture Fed Wideband Circularly Polarized Rectangular Stair Shaped Dielectric Resonator Antenna. *IEEE Trans. Antennas Propag.* **54**, 1350-1352 (2006).

12. Khoo, K. W., Guo, Y. X. & Ong, L. C. Wideband Circularly Polarized Dielectric Resonator Antenna. *IEEE Trans. Antennas Propag.* **55**, 1929-1932 (2007).

13. Pan, Y. & Leung, K. W. Wideband circularly polarized trapezoidal dielectric resonator antenna. *IEEE Antennas Wirel. Propag. Lett.* **9**, 588–591 (2010).

14. Khalily, M., Kamarudin, M. R. & Jamaluddin, M. H. A novel square dielectric resonator antenna with two unequal inclined slits for wideband circular polarization. *IEEE Antennas Wirel. Propag. Lett.* **12**, 1256–1259 (2013).

15. Zou, M., Pan, J. & Nie, Z. A Wideband Circularly Polarized Rectangular Dielectric Resonator Antenna Excited by an Archimedean Spiral Slot *IEEE Antennas Wirel. Propag. Lett.* **14**, 446–449 (2015).

16. Illahi, U., Iqbal, J., Sulaiman, M. I., Alam, M. M.,Su'ud, M. M. & Jamaluddin, M. H. Singly-Fed Rectangular Dielectric Resonator Antenna with a Wide Circular Polarization Bandwidth and Beamwidth for WiMAX/Satellite Applications. *IEEE Access* **7**, 66206-66214 (2019).

17. Yang, M., Pan, Y. & Yang, W. A Singly Fed Wideband Circularly Polarized Dielectric Resonator Antenna. *IEEE Antennas Wirel. Propag. Lett.* **17**, 1515-1518 (2018).

18. Abedian, M., Rahim, S. K. A., Danesh, S., Jamaluddin, M. H. & Islam, M. T. Compact wideband circularly polarised dielectric resonator antenna. *Electron. Lett.* **53**, 5-6 (2017).

19. Varshney, G., Pandey, V. S., Yaduvanshi, R. S. & Kumar, L. Wide Band Circularly Polarized Dielectric Resonator Antenna with Stair-Shaped Slot Excitation. *IEEE Trans. Antennas Propag.* **65**, 1380-1383 (2017).

20. Chowdhury, R., Mishra, N., Sani, M. M. & Chaudhary, R. K. Analysis of a Wideband Circularly Polarized Cylindrical Dielectric Resonator Antenna with Broadside Radiation Coupled with Simple Microstrip Feeding. *IEEE Access* **5**, 19478-19485 (2017).

21. Kumar, B. P., Guha, D. & Kumar, C. Reduction of Beam Squinting and Cross-Polarized Fields in a Wideband CP Element. *IEEE Antennas Wirel. Propag. Lett.* **19**, 418-422 (2020).

22. Kumar, R. & Chaudhary, R. K. A Wideband Circularly Polarized Cubic Dielectric Resonator Antenna Excited with Modified Microstrip Feed. *IEEE Antennas Wirel. Propag. Lett.* **15**, 1285-1288 (2016).

23. Altaf, A., Yang, Y., Lee, K. & Hwang, K. C. Circularly Polarized Spidron Fractal Dielectric Resonator Antenna. *IEEE Antennas Wirel. Propag. Lett.* **14**, 1806-1809 (2015).

24. Sulaiman, M. I. & Khamas, S. K. A Singly Fed Wideband Circularly Polarized Dielectric Resonator Antenna Using Concentric Open Half-Loops. *IEEE Antennas Wirel. Propag. Lett.* **10**, 1305-1308 (2011).

25. Rashidian, A., Shafai, L. & Klymyshyn, D. M. Compact Wideband Multimode Dielectric Resonator Antennas Fed with Parallel Standing Strips. *IEEE Trans. Antennas Propag.* **60**, 5021-5031 (2012).

Figures

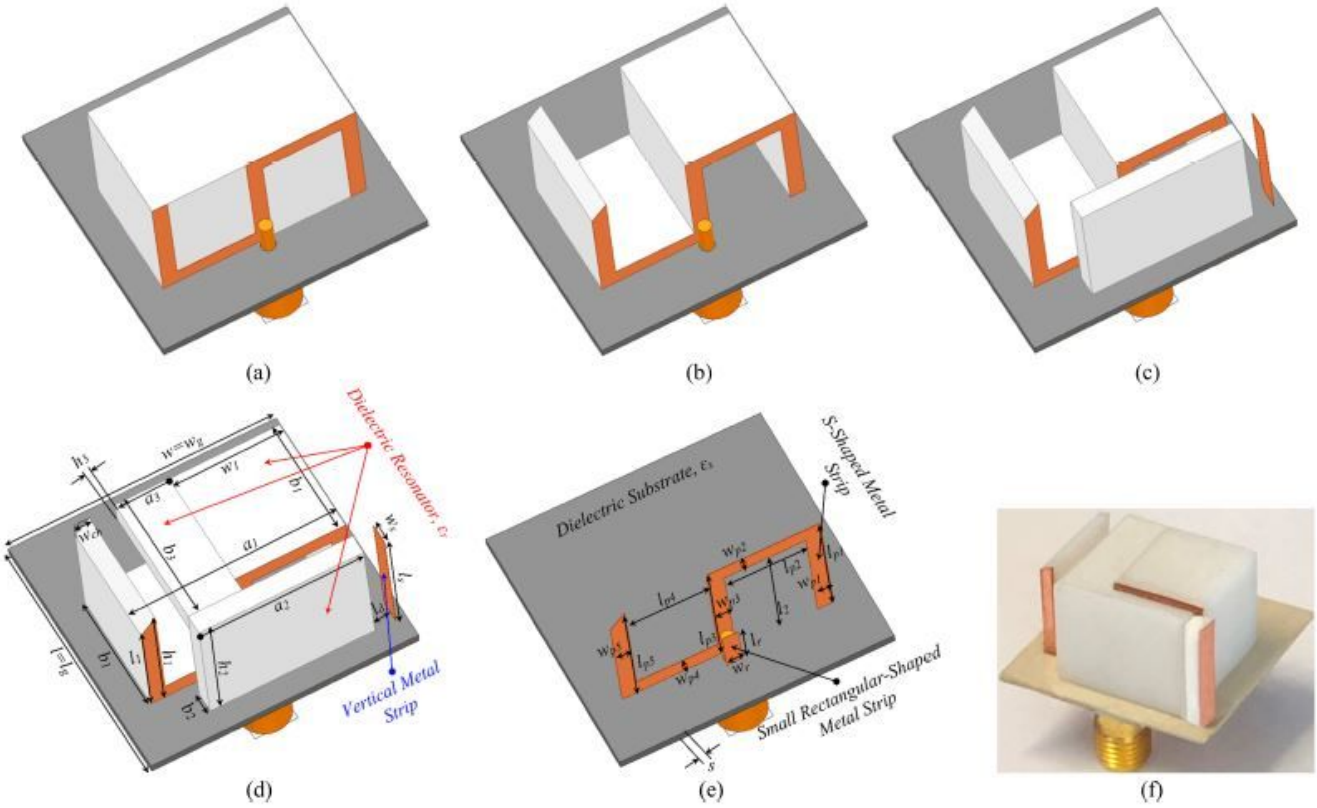

Figure 1

Evolution of the proposed CP DRA: (a) RDRA, (b) SDRA (Antenna I), (c) SDRA with the first added RDR and vertical metal strip (Antenna II), (d) SDRA with the first and the second added RDRs (Antenna III); Geometry of the proposed CP DRA, (e) feeding mechanism, and (f) the prototype of proposed DRA. (l = lg = 26, w = wg = 26, lp1 = lp3 = lp5 = 12, lp2 = lp4 = 7.75, wp1 = wp3 = wp5 = 1.5, wp2 = wp4 = 2, lr = 4, wr = 2, ls = 12, ws = 2, ld = 2, wch = 1.5, l1 = 10.5, l2 = 10, w1 = 10.75, a1 = 20, b1 = 12, h1 = 12, a2 = 16, b2 = 2, h2 = 12, a3 = 5.25, b3 = 13.345, h3 = 2, er = 10, es = 3, = 0.75. Unit : mm).

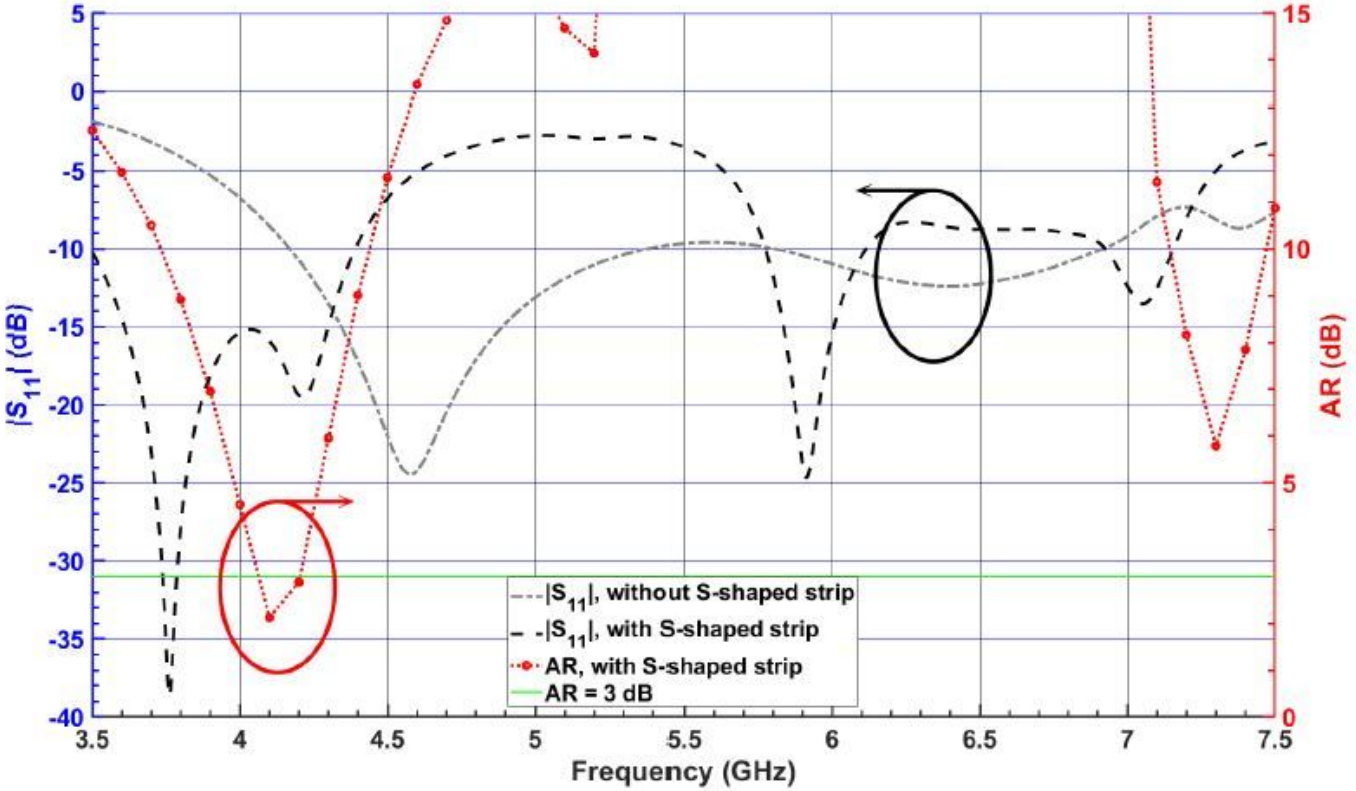

Figure 2

Simulated |S11| and AR of the RDRA with and without an S-shaped metal strip.

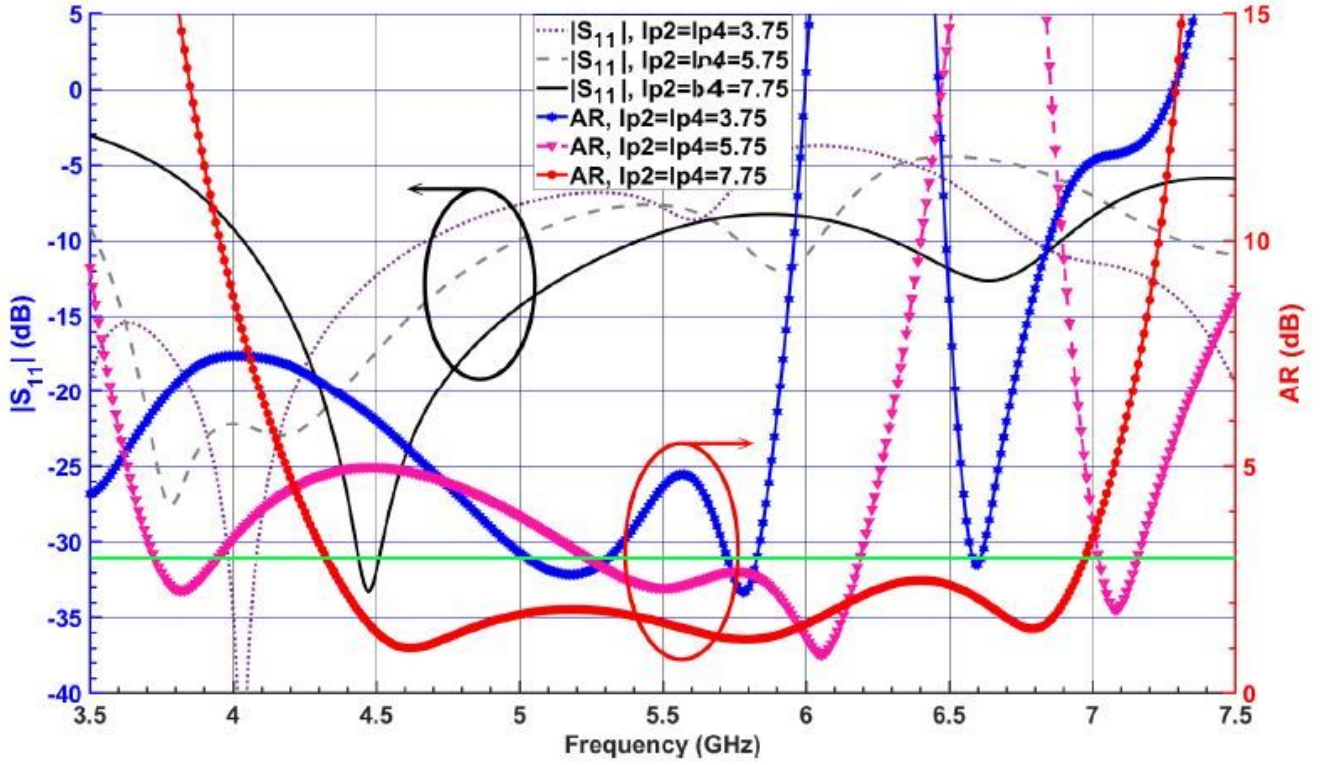

Figure 3

Simulated |S11| and ARs of the SDRA with different values of lp2 = lp4.

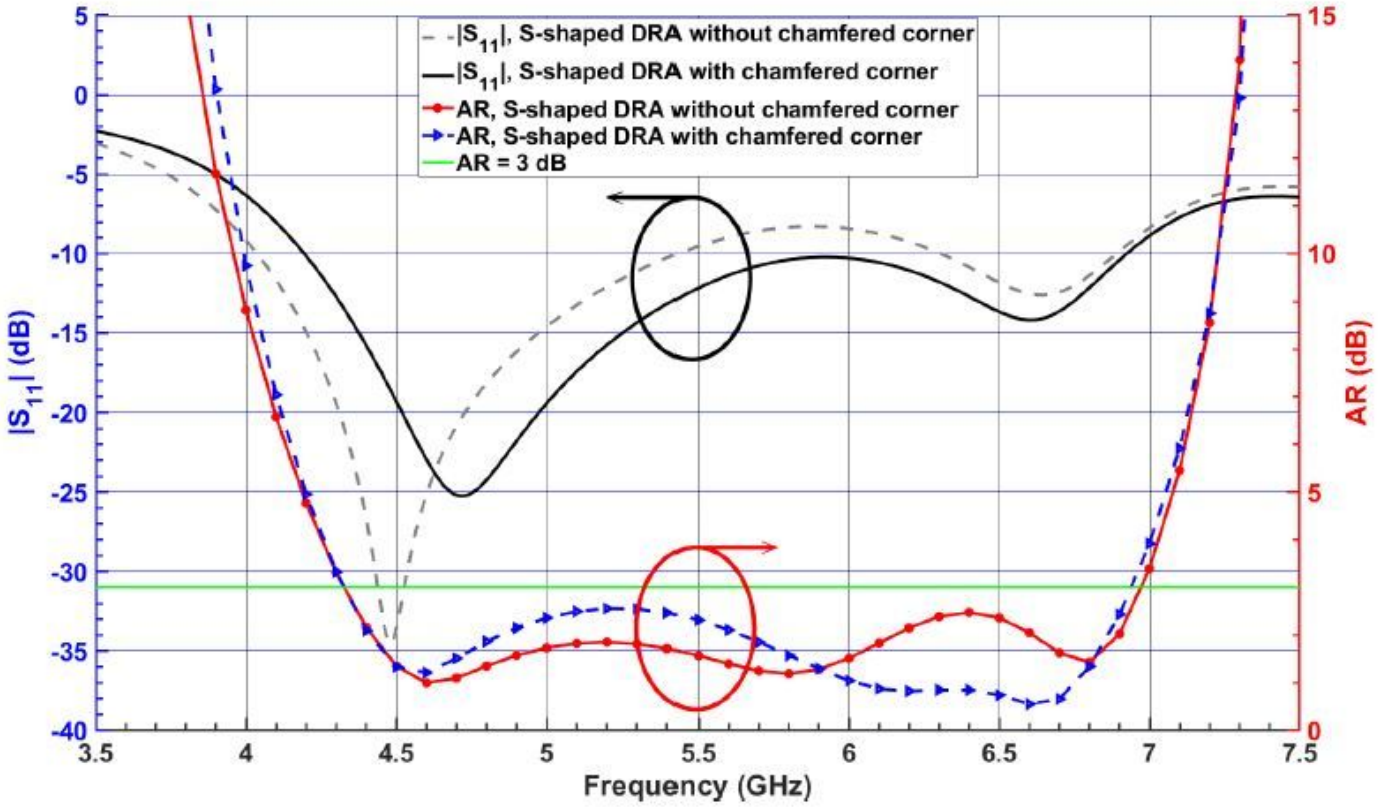

Figure 4

Simulated |S11| and ARs of the SDRA with and without chamfered corner.

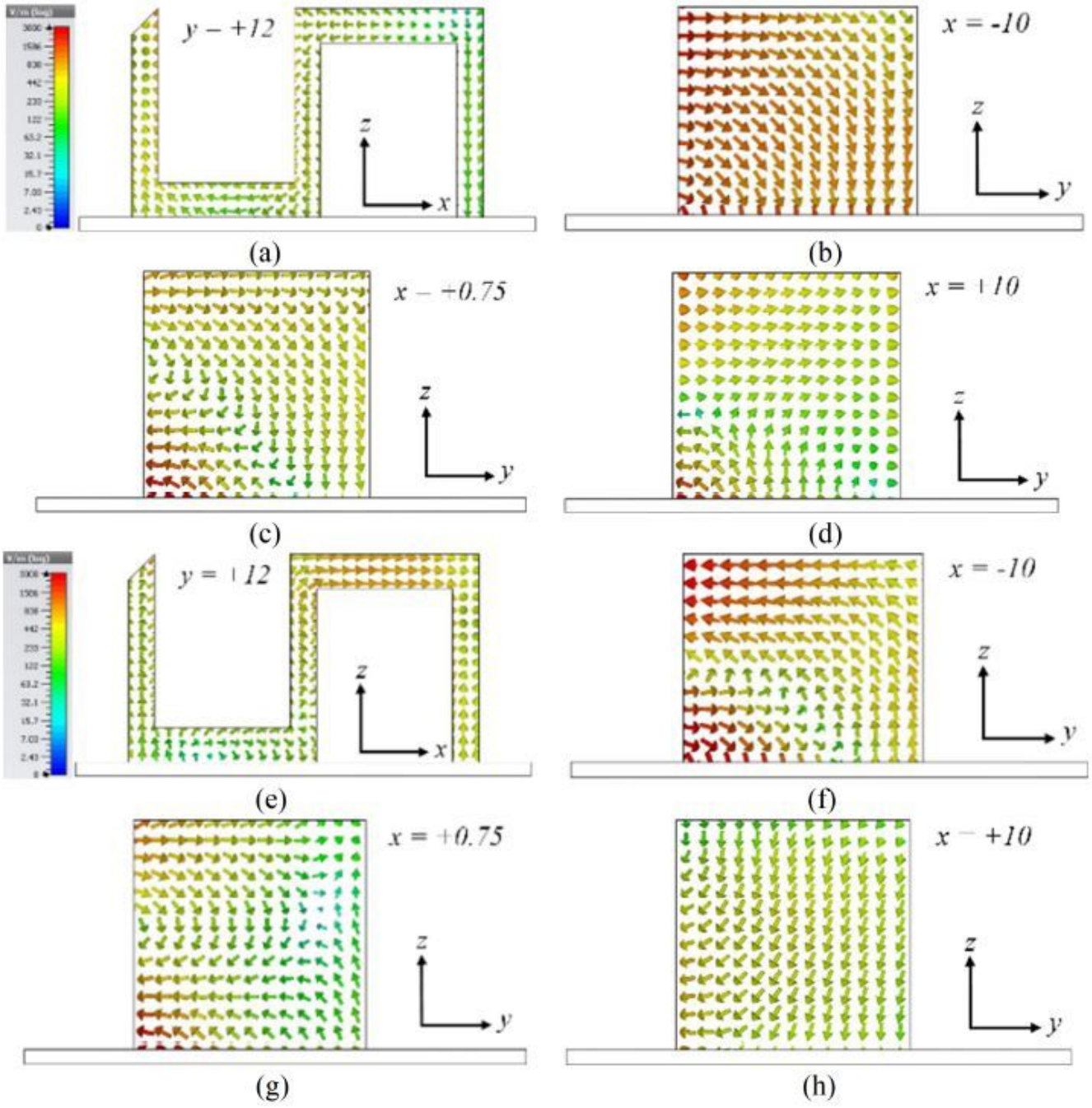

Figure 5

Simulated electric field vectors on different surfaces of the SDR; at 4:6 GHz (a) 45° (y = 12mm), (b) 135 (x = -10), (c) 135° (x = +0.75), and (d) 135° (x = +10); at 6:5 GHz (e) 45° (y = 12mm), (f) 135° (x = -10), (g) 135° (x = +0.75), and (h) 135° (x = +10); (color bar shows the amplitude of the E-field.

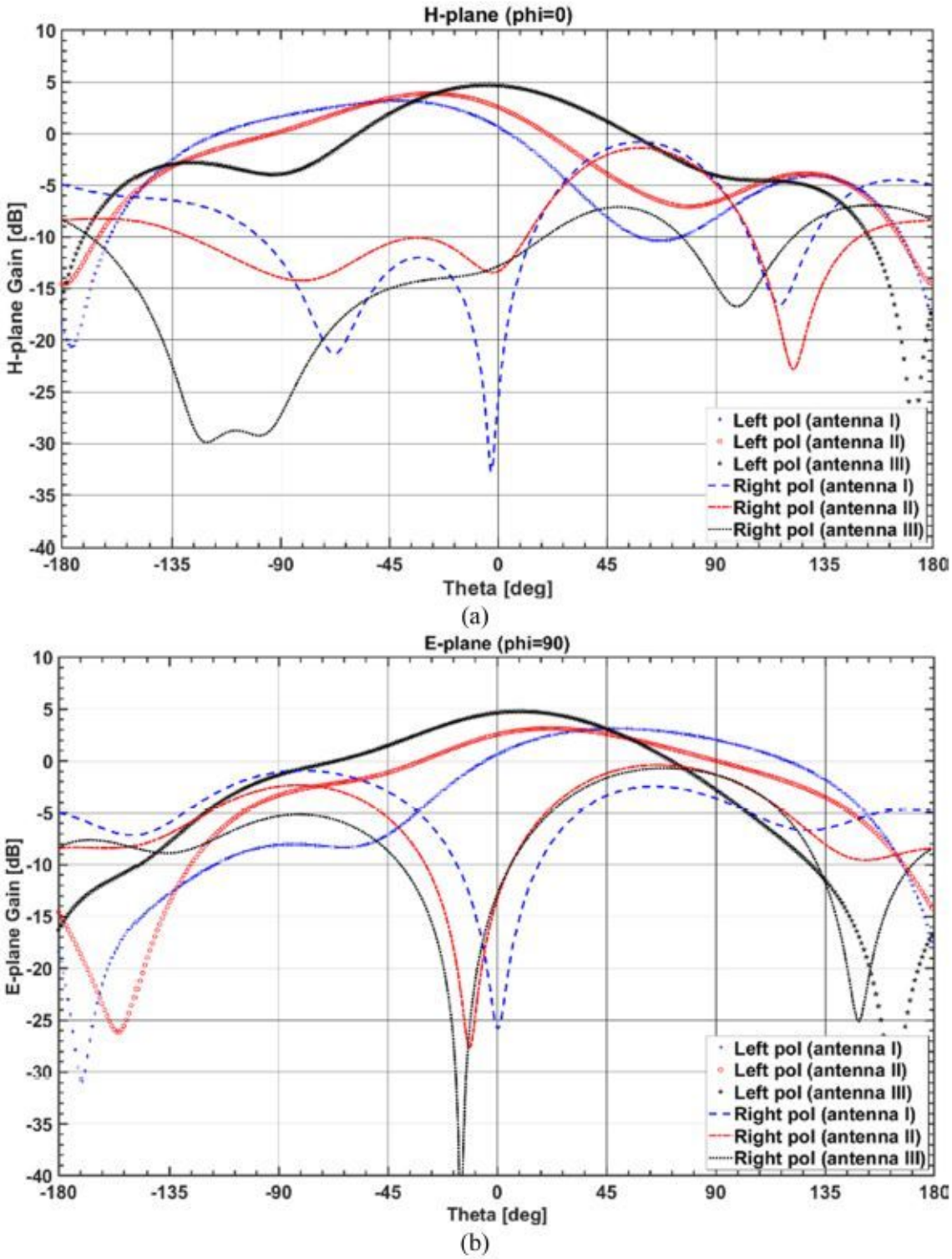

Figure 6

Simulated (a) H-plane and (b) E-plane radiation patterns of Antenna I, Antenna II, and Antenna III at 6:5 GHz.

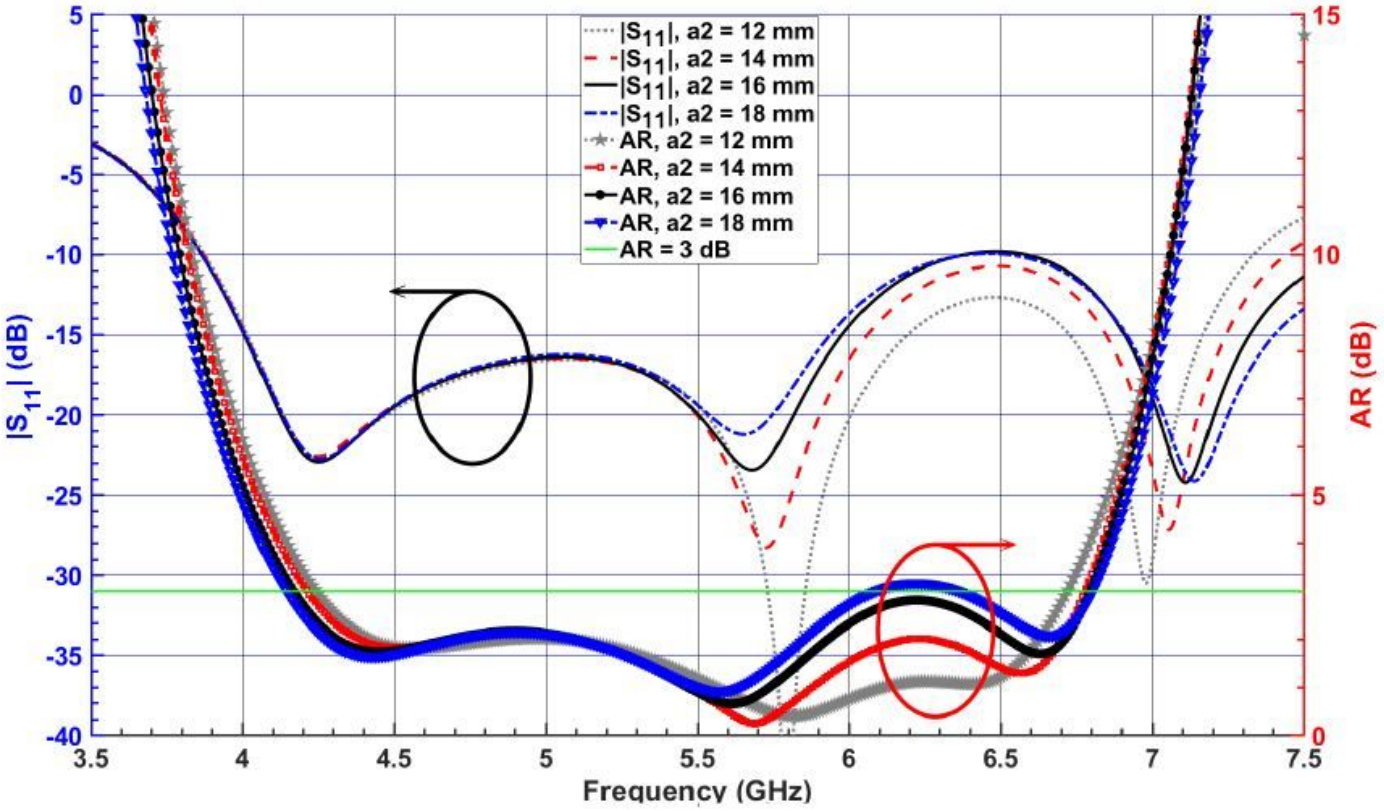

Figure 7

Simulated |S11| and ARs for the DRA (Antenna II) versus various total lengths α2 of the first added RD.

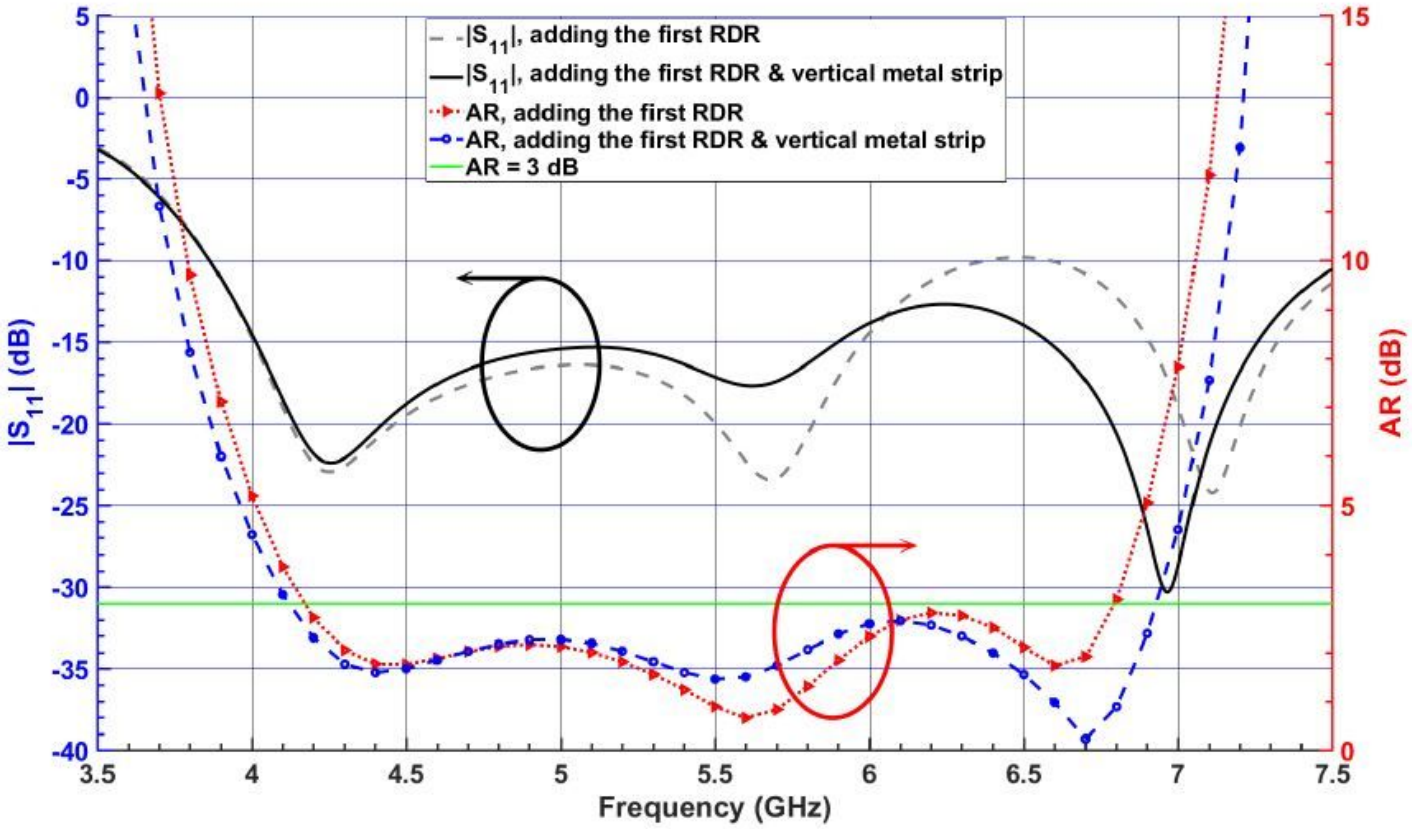

Figure 8

Simulated |S11| and ARs of the DRA (Antenna II), adding the first RDR block and vertical metal strip.

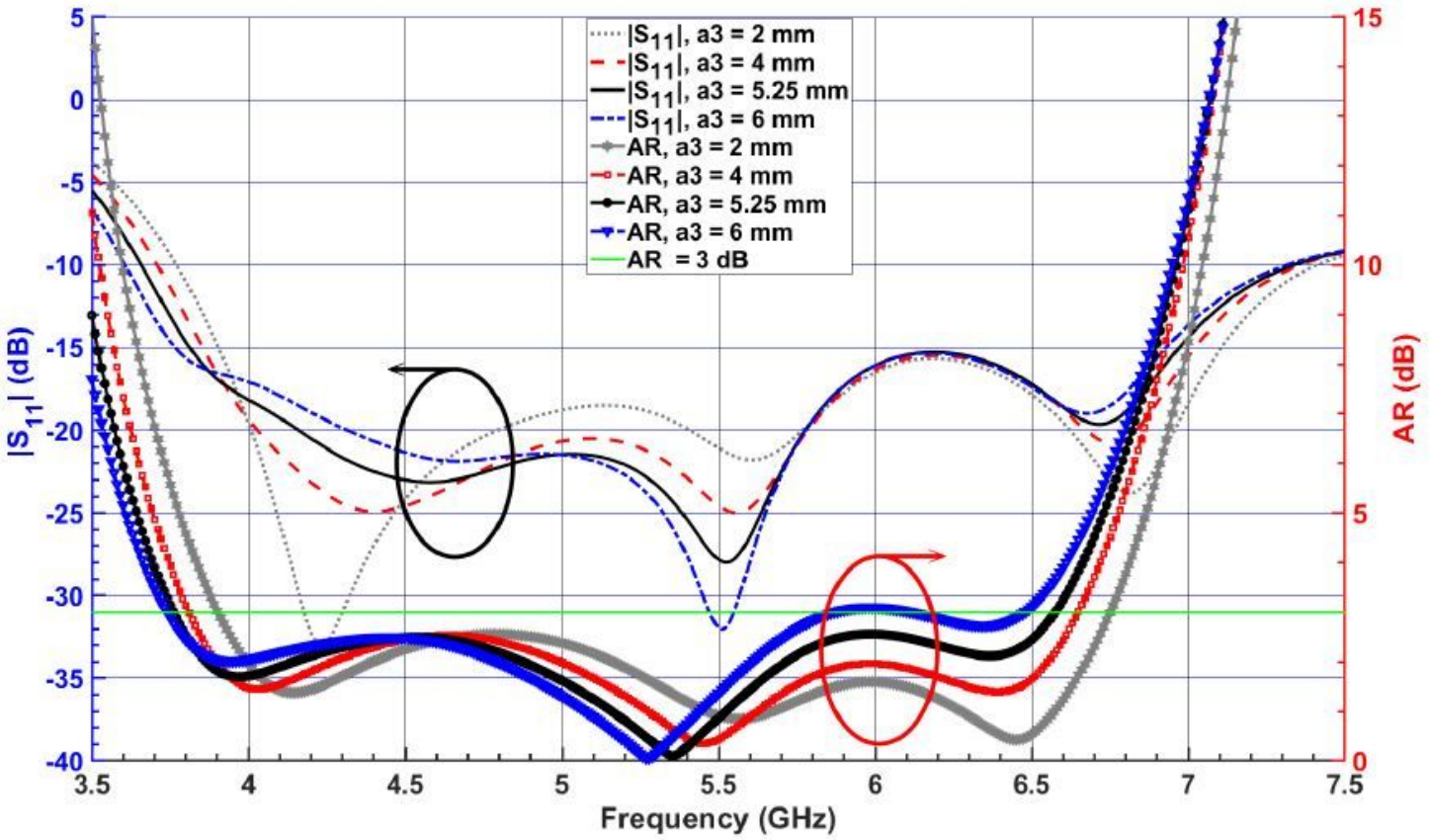

Figure 9

Simulated |S11| and ARs for the DRA (Antenna III) with various total widths α3 of the second added RDR.

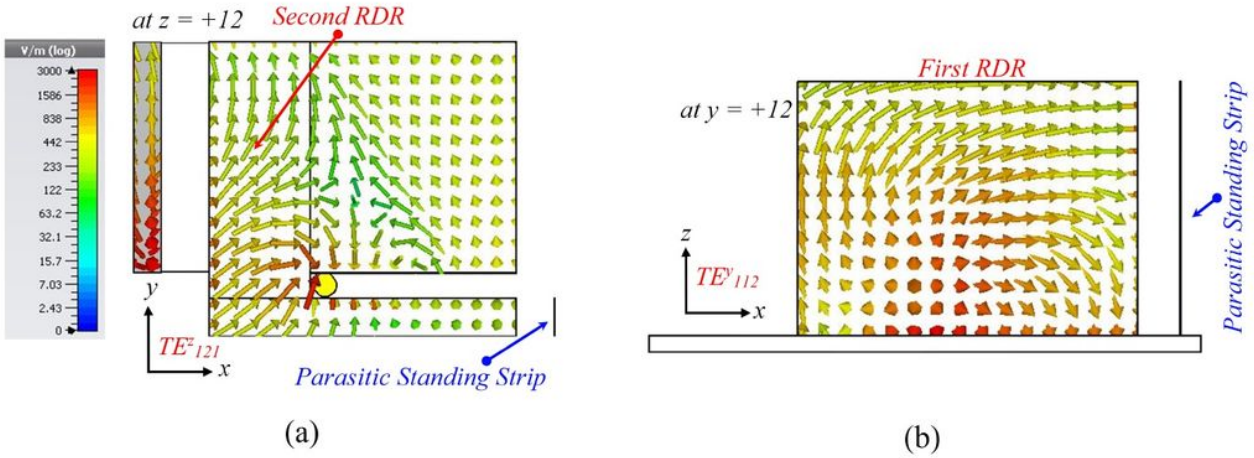

Figure 10

Simulated electric field vectors on the top surface of the SDR and the vertical surface of the first RDR at 5.5 GHz (a) xy-plane 0° (z = 12mm), (b) xz-plane 90° (y = 12mm); (color bar shows the amplitude of the E-field).

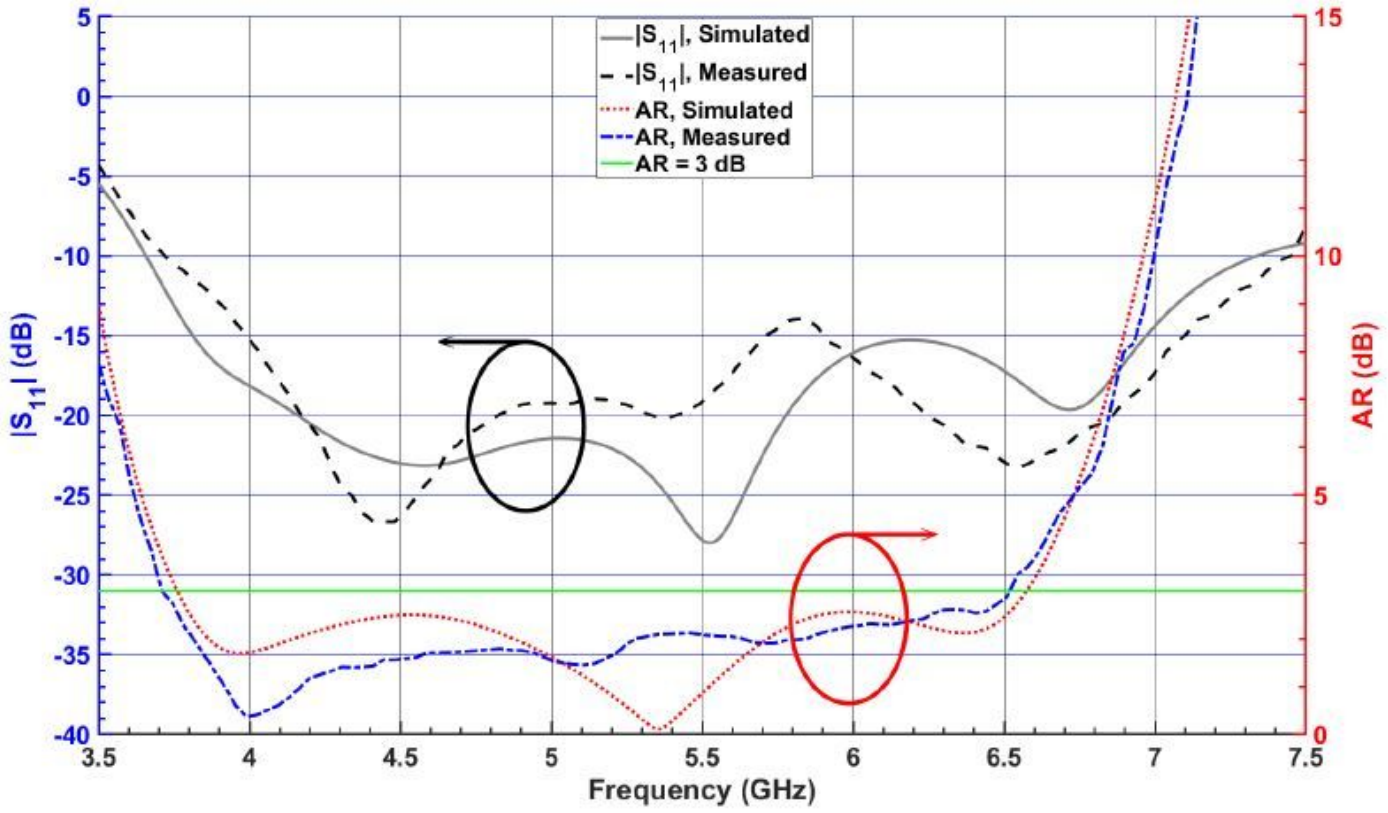

Figure 11

Simulated and measured jS11j and ARs of the proposed CP DRA.

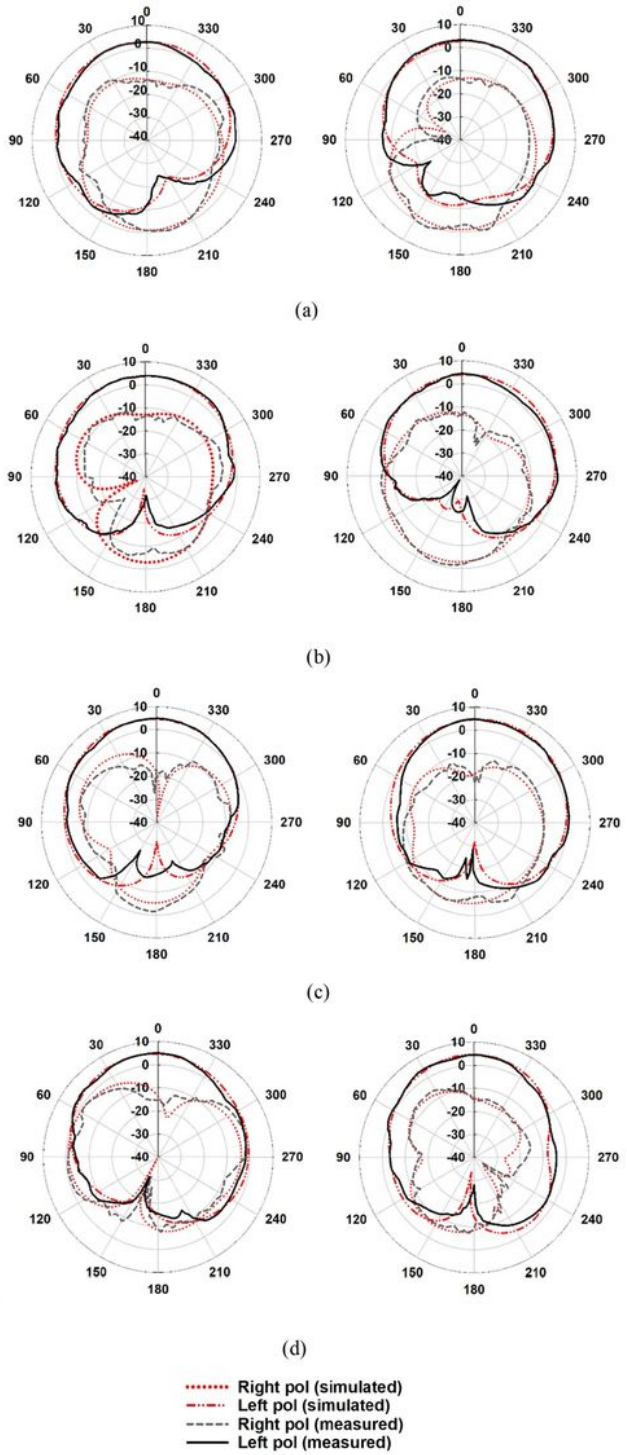

Figure 12

Simulated and measured LHCP and RHCP radiation patterns in xz-plane (left) and yz-plane (right) at (a) 3:76 GHz, (b) 4:6 GHz, (c) 5:5 GHz, and (d) 6:5 GHz. Red and black curves represent simulated and measured results, respectively.

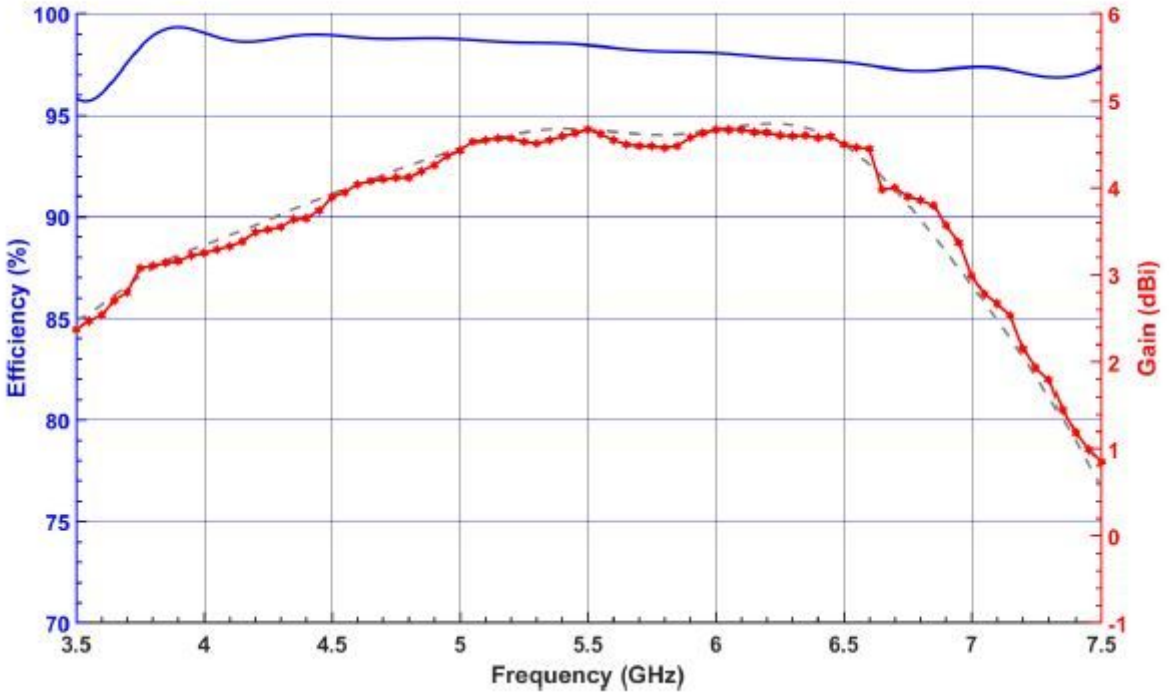

Figure 13

Measured and simulated boresight gain of the proposed CP-DRA and simulated radiation efficiency